Dalton Transactions

ROYAL SOCIETY OF CHEMISTRY

PAPER

View Article Online
View Journal | View Issue

Check for updates

Cite this: *Dalton Trans.*, 2024, **53**, 18932

Synthesis and characterization of NiAl-hydride heterometallics: perturbing electron density within Al–H–Ni subunits†

Aleida G. Gonzalez,[a] Fernando Gonzalez,[a] Edgardo De Leon,[a] Kaitlyn M. Birkhoff,[b] Sam Yruegas,[b] Haoyuan Chen*[c,d] and Manar M. Shoshani*[a,e]

Received 19th June 2024,
Accepted 19th August 2024

DOI: 10.1039/d4dt01786b

rsc.li/dalton

Heterometallic hydride complexes are of growing interest due to their potential to contribute to highly active insertion-based catalysis; however, methods to modulate electron density within this class of molecules are underexplored. Addition of ancillary ligands to heterotrimetallic $NiAl_2H_2$ species (**1**) results in the formation of heterobimetallic NiAl-hydride complexes with varying phosphine donors (**2-(L)$_2$**). Incorporation of sigma donating ancillary ligands of increasing strength led to contractions of the Ni–Al distances correlated to a strengthening of a back donation interaction to the Al–H sigma antibonding orbital, most prominently present in **2-(PMe$_3$)$_2$**. Demethylation of the aryl ether from **2-(PMe$_3$)$_2$** provides access to a novel anionic nickel–aluminum complex (**3**) with a maintained bridged hydride moiety between Ni and Al. Increased negative charge in complex **3** results in an elongation of the Ni–Al interaction. Combined crystallographic, spectroscopic, and computational studies support a 3-center interaction within the Al–H–Ni subunits and were used to map the degree of Ni–H character of the series within the Al–H–Ni bonding continuum.

Introduction

Heterometallic complexes bearing redox-active and redox-inactive metal centers have been of growing interest over the past few decades.[1,2] This interest is, in part, correlated to the desire to impart cooperative reactivity towards organic substrates which is predominantly described through either (1) a redox-inactive metal coordinating and guiding substrates to further activation and functionalization at the transition metal center, or (2) the redox inactive metal center binding directly to the transition metal as a sigma acceptor to generate a more electrophilic transition metal center.[3,4] Both modes of cooperativity have been well-documented and have led to progress in a multitude of noteworthy reactions including, but not limited to, N-heterocycle C–H activation,[5] CO_2 reduction,[6–8] olefin hydrogenation,[9] and dihydrogen activation.[10,11] Reactivity by incorporating transition metals and Lewis-acidic metalloid boron in a single system has shown a wide array of success in bond activation and catalysis.[12–16]

The intermediacy of metal-hydrides in a plethora of catalytic cycles is widely acknowledged[17] and multimetallic hydride moieties, specifically, are responsible for a multitude of impressive bond transformations.[18] Indeed within homogenous catalysis, examples with late transition metals and main group hydride additives have exhibited success in inert-bond activation; yet the ill-defined nature of the reaction conditions limits the mechanistic insight one can glean in relation to cooperative reactivity.[19] Examples of reactivity from well-defined heterometallic hydride complexes are still emerging[20] which is, in part, due to synthetic challenges in accessing well-defined heterometallic hydride complexes with discrete nuclearity. Moreover, reliance on the self-assembly of metal ions on ligands to generate related species continues to impede progress.[21–23] Dependence on monodentate ligands in this domain offers poor control over nuclearity of multimetallic hydride complexes.[24] Complexes including precious metals such as Rh and Ir with bridging aluminum hydrides are known,[25–27] as well as recent examples with base metals.[28,29]

[a]*School of Integrated Biological and Chemical Sciences, University of Texas Rio Grande Valley, Brownsville, Texas, 78520, USA*
[b]*Department of Chemistry, Rice University, Houston, Texas, 77005, USA*
[c]*Department of Physics and Astronomy, University of Texas Rio Grande Valley, Edinburg, Texas, 78539, USA*
[d]*Department of Chemistry, Southern Methodist University, Dallas, Texas, 75275, USA. E-mail: haoyuan@smu.edu*
[e]*Department of Chemistry, University of Kansas, Lawrence, Kansas, 66045, USA. E-mail: manar.shoshani@ku.edu*

†Electronic supplementary information (ESI) available. CCDC 2362005, 2362006, 2362008 and 2362009. For ESI and crystallographic data in CIF or other electronic format see DOI: https://doi.org/10.1039/d4dt01786b

Given the dearth of examples where the hydride moieties are bridged between heterometallic centers, studies on electronic structure to better understand the impact of generating heterometallic complexes of this sort are limited. Fortunately, examples of well-defined heterometallic hydrides of this nature have been reported recently, select examples are shown in Fig. 1. Complex **I** features a trimetallic Ni–Mg complex with 4 bridged hydrides by Xu *et al.*, capable of catalytic insertion chemistry with unsaturated substrates.[30,31] Complexes **II** and **III** by the Crimmin group employ main group beta-diketiminate moieties to bridge Al and Mg hydrides to Fe and Pd centers, respectively.[32–34] The electronic structure of these complexes has been thoroughly studied to gain an understanding of the nature of the heterometallic subunits. Complex **II** is reported to facilitate *ortho*-directed C–H bond activation of N-heterocycles.

Examples with bridging hydrides between Ni and Al centers are highly limited; complexes **IV**, **V**, **VI** are the currently reported crystallographically characterized examples by other groups.[35–37] Developing a thorough understanding of the capability of heterometallic hydrides, transcending the classical substrate preactivation and directing nature is crucial. Recently, facile anionic group transfer was reported for transition metal-aluminum containing species, including halides, alkyls, and hydride transfers.[38] Complex **VII** is a rare report of an Al–H–Ni generated *in situ via* addition of dihydrogen to a nickel-alane complex.[39] The system demonstrates facile reversibility between alane and aluminyl states through auxiliary substrate coordination. The system used in complex **VII** outlines potential novel pathways for future reactivity leveraging Lewis-acidic metals in redox activity and electron storage.

Our group recently reported complex **1**, a $NiAl_2H_2$ catalyst capable of hydrofunctionalization of N-heterocycles.[40] Complex **1** exhibits a markable increase in activity of hydrofunctionalization catalysis in comparison to the alane precursor which underscores the crucial nature of generating multimetallic hydrides to amplify insertion-based reactivity. In the interest of delineating the bonding picture in complexes related to the examples in Fig. 1a, Fig. 1b demonstrates a scale that denotes the extremes of the bonding continuum within the Al–H–Ni subunit of complex **1**, ranging from an Al–H alane to a Ni–H with a highly sigma-donating and *trans*-influencing aluminyl moiety.[41] While complex **1** lies somewhere in between the extremes, and there are accompanying parameters that offer guidance such as the Ni–Al distances and the geometry at Ni, further investigations towards understanding how to quantify or designate complexes within the context of the scale are needed. Indeed, the groups of Aldridge and Crimmin have thoroughly studied transition metal-main group hydride complexes, including examples of transition metal-alanes, and

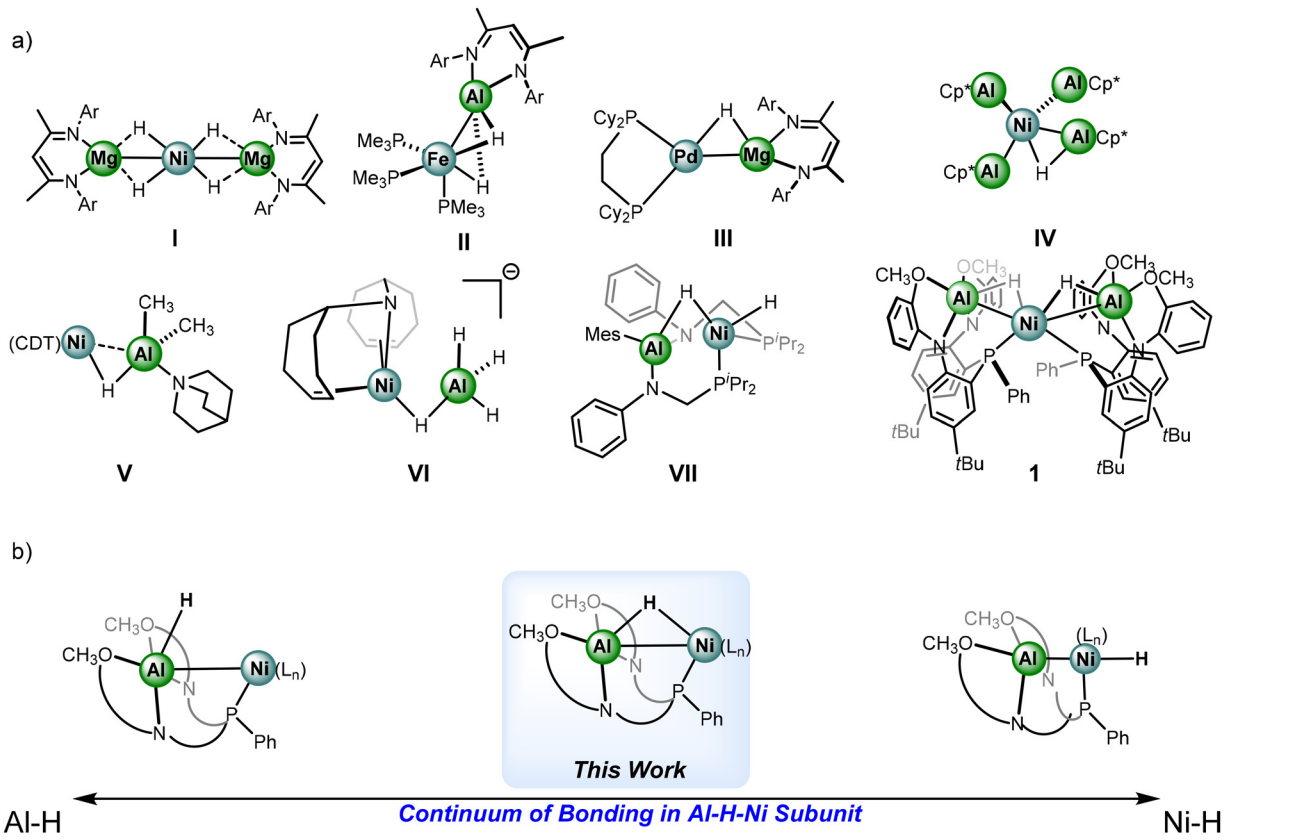

Fig. 1 (a) Select examples of heterometallic hydride complexes with first row transition metals. (b) Extremes of sigma bonding within an Al–H and Ni–H.

have provided a blueprint in assessing degrees of activation within main group hydrides.[42,43] The interactions are described through the Dewar–Chatt–Duncanson model where the main group hydride fragment donates electron density to an empty d-orbital and back donation from a filled d_π-orbital to an Al–H sigma-antibonding orbital;[27,44] notably the latter interaction has been described a minimal contributor in a series of reported examples.[45] Given the lack of known examples featuring an Al–H–Ni subunit, and their growing interest given potential in catalysis, further work is needed to elucidate the electronic structure.[46] Herein, we discuss the synthesis of new heterometallic complexes with an Al–H–Ni subunit and efforts to perturb and monitor the electron density distribution within the framework.

Results and discussion

Synthesis and characterization of neutral NiAl heterobimetallic hydride complexes

In the solid-state, complex **1** features a Ni center supported by two phosphine donors of the metalloligands as well as two Al–H fragments, the latter in a 3-center bonding motif. Our group desired to explore the continuum by probing complex **1** through examining the impact of addition of ancillary ligands to the primary coordination sphere and monitoring the impact in electronic structure.

We envisioned the fate of the coordination site of the added ancillary ligands may be instructive to the nature of the hydride moiety, specifically towards where on the continuum of sigma-binding the hydride of derivatives of complex **1** resides. For instance, addition of an ancillary ligand (L) to complex **1** could result in coordination of L at Ni to generate an Ni-alane with greater Al–H character (**A** – Scheme 1). Alternatively, L could coordinate to Al and subsequently result in the formation of a species with greater Ni hydride character and a coordinated aluminyl center (**B** – Scheme 1), analogous to anionic group transfers reported by Lu *et al.*[39] As discussed above, access to Ni-aluminyl complexes has been recently shown to be relatively facile and the rules that govern interconversion are of growing interest. In the event of pathway B, the retention of the trimetallic core would hinder a *trans* arrangement of the hydride moiety to the aluminyl. Additionally, ancillary ligands could also result in dissociation of the metalloligand itself to form heterobimetallic complexes (**C** – Scheme 1). Though option C provides the least decisive description towards the nature of the hydride moiety, one can still glean relevant information based on the comparative electronic properties of the ancillary ligand, and the impact towards the Al–H–Ni subunit.

Given that addition of $Ni(COD)_2$ to metalloligand LAlH results in the formation of complex **1**, rather than a COD-coordinated species, ancillary ligands serving as strong sigma donors were pursued in our study. Addition of excess triphenylphosphine to complex **1** produces a new complex

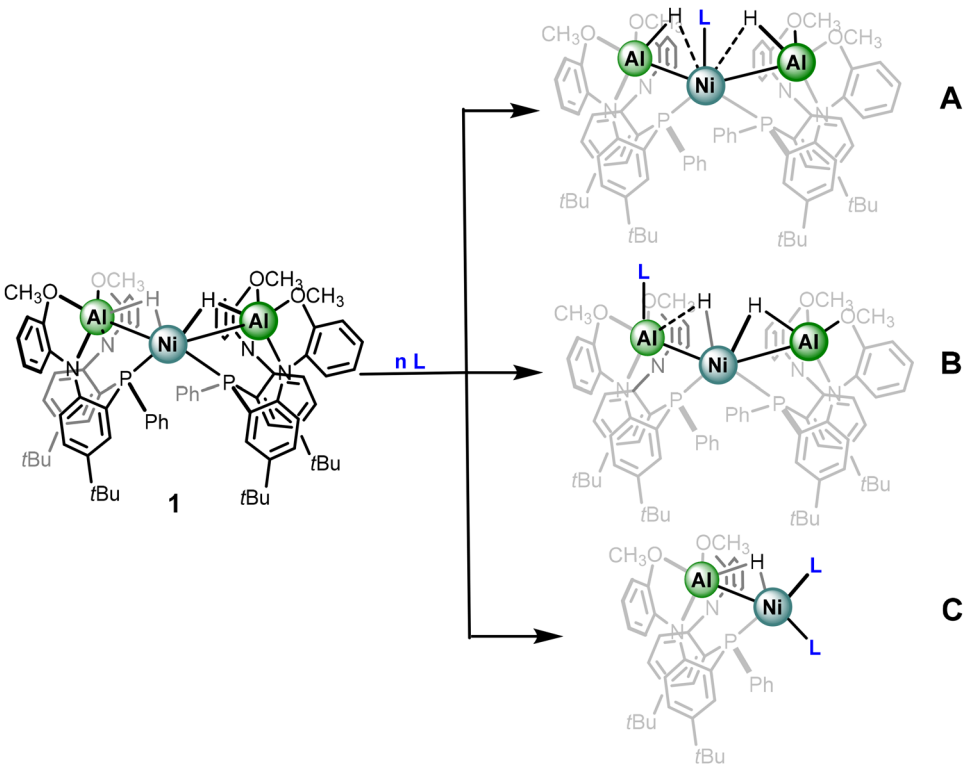

Scheme 1 Potential coordination sites of ancillary ligands to complex **1**.

bearing a $^{31}P\{^{1}H\}$ NMR spectrum consistent with a heterometallic complex with two triphenyl phosphine ligands and one metalloligand, indicating the formation of the heterobimetallic species **2-(PPh$_3$)$_2$** (Scheme 2). Specifically, a triplet at δ −12.48 corresponding to the metalloligand phosphine and a broad resonance at δ 29.26 are observed. The latter resonance sharpens to a doublet at 55 °C with corresponding coupling constants of 9.6 Hz. Both ^{1}H and $^{13}C\{^{1}H\}$ NMR spectra are consistent with the formation of a heterobimetallic hydride complex including the observation of a hydride resonance at δ −1.78, a slight upfield shift from the hydride resonance of complex **1**. The resonance appears as a broad doublet J_{HP} of 53.3 Hz, which is consistent with the multiplicity of complex **1**. While the expectation is to observe a doublet of triplets from additional coupling to the phosphorus centers of the triphenylphosphine moieties, it is likely that the broadening from coupling to quadrupolar ^{27}Al obfuscates observation of further coupling. Exposing complex **1** to conditions to balance the reaction, including four equivalents of PPh_3 and one equivalent of $Ni(COD)_2$ results in quantitative conversion to **2-(PPh$_3$)$_2$**. Separately, conditions were identified to synthesize **2-(PPh$_3$)$_2$** directly from the LAlH precursor (Scheme 2).

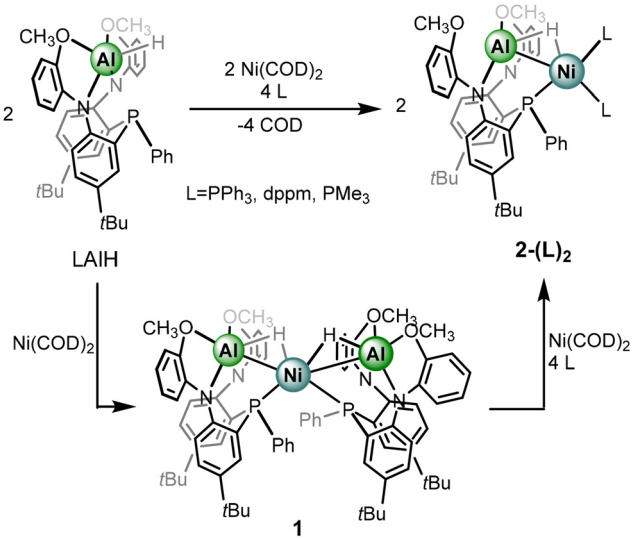

Scheme 2 Synthesis of complexes **2-(L)$_2$**.

The solid-state structure of **2-(PPh$_3$)$_2$** was obtained by single-crystal X-ray diffraction and features several noteworthy features (Fig. 2a). The heterobimetallic features a Ni–Al distance of 2.322(1) Å, representing a contraction compared to the Ni–Al distance of 2.363(3) Å in complex **1**. The shortening is reasoned through a strengthening of the Ni–Al interaction as the two PPh_3 ligands may serve as more electron donating in comparison to the metalloligand in **1**. As a result, a more electron rich Ni center would be better equipped to donate to the Al–H sigma antibonding orbital. Furthermore, in **2-(PPh$_3$)$_2$** only one of the methoxy groups is coordinated to the Al center which may be the result of the Ni–Al interaction strengthening and the Lewis-acidic Al center requiring less coordinative stabilization. However, the ^{1}H NMR data features only one methoxy resonance which could indicate a fast exchange of methoxy coordination to Al, or that in solution, both donors are coordinated. The hydride ligand was located on the electron difference map and indicates that the bridged nature between the Ni and Al centers is maintained. The Ni–H distances are comparable to that of **1** but the Al–H distance shows a slight elongation; however, the crystallographically determined M–H distances provide limited insight. With respect to the hydride ligand and the three phosphine donors, a τ'_4 [47] value of 0.92 about Ni is calculated which is consistent with tetrahedral geometry, expected for a Ni-alane, rather than square planar geometry for a Ni-hydride-aluminyl. However, given the sigma-complex bonding assignment, determining the τ value from bond angles at some point along the Al–H bond rather than the hydride center itself is more appropriate. Nevertheless, a

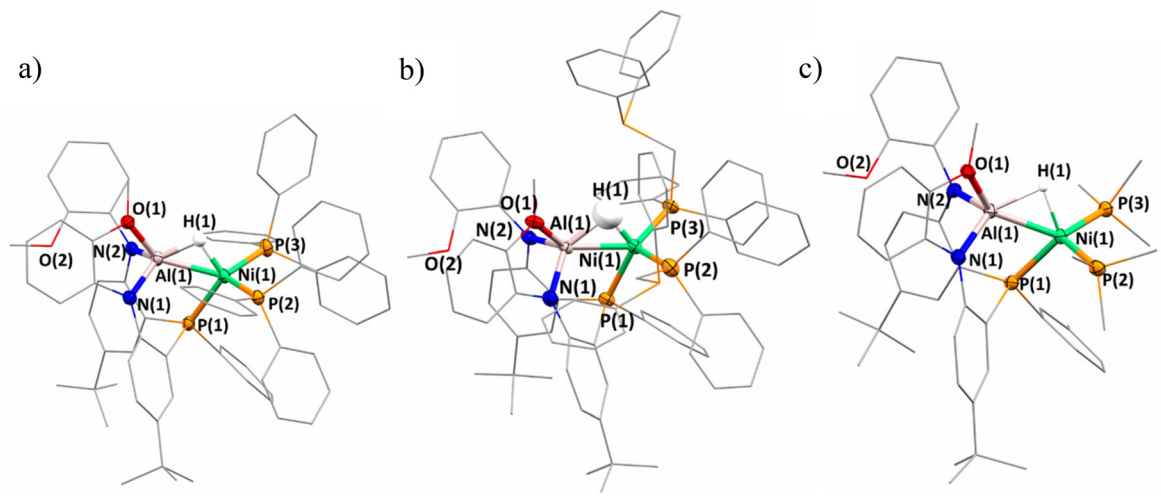

Fig. 2 Solid-state structures of (a) **2-(PPh$_3$)$_2$**, (b) **2-(dppm)$_2$**, and (c) **2-(PMe$_3$)$_2$**. Hydrogen atoms on ligands are excluded for clarity. Mixed wireframe/ellipsoid view used for clarity.

distorted tetrahedral geometry is the most appropriate descriptor for Ni in **2-(PPh$_3$)$_2$**. The impact on electron count and oxidation state by sigma-acceptors has been discussed at length elsewhere.[48,49] Though option **C** from Scheme 1 seems to dominate when L = PPh_3, examining the consistency of this result with further ancillary ligands to potentially probe the Al center for coordination, as well as further interrogating the impact of the Al–H–Ni subunit *via* coordination at the Ni site, became of increased interest.

The chelating phosphine, bis-diphenylphosphinomethane (dppm) was employed as an auxiliary donor. We sought to explore whether the phosphine centers would serve as a chelate between Ni and Al, bind one equivalent to the Ni or Al centers in a chelating fashion, or coordinate two equivalents at Ni in a terminal fashion, akin to **2-(PPh$_3$)$_2$**.[50] Indeed, addition of dppm to complex **1** along with $Ni(COD)_2$ quantitatively formed the heterometallic analogue, **2-(dppm)$_2$** with the phosphine ligands coordinating in a non-chelate fashion. Similar to **2-(PPh$_3$)$_2$**, complex **2-(dppm)$_2$** is preferentially and reasonably synthesized directly from metalloligand LAlH. Complex **2-(dppm)$_2$** features three resonances in the $^{31}P\{^1H\}$ NMR spectrum: a triplet at δ −12.35, a corresponding doublet at δ −27.05, and a broad resonance at δ 20.72 integrating in a 1 : 2 : 2 ratio, respectively. The triplet and doublet resonances correspond to the phosphorus centers in the coordination sphere of Ni, the triplet belonging to the metalloligand phosphorus center and doublet to the bound dppm phosphorus center. Lastly, the broad resonance corresponds to the unbound dppm phosphorus centers. Variable-temperature $^{31}P\{^1H\}$ NMR was employed and displays decoalescence of both dppm resonances at −20 °C amounting to a total of 5 resonances for complex **2-(dppm)$_2$** (Fig. S2 and S3†). The $^{31}P\{^1H\}$ NMR spectrum at 60 °C exhibits sharpening of all resonances as well as resolving of coupling features (Fig. S2 and S4†). The ^1H NMR spectrum shows the presence of the bridged hydride at δ −2.10, which once again appears as a broad doublet and is slightly upfield in comparison to the hydride resonance in **1** and **2-(PPh$_3$)$_2$**.

The solid-state structure confirms the solution-state assignment demonstrating that **2-(dppm)$_2$** (Fig. 2b) features a heterobimetallic core with two dppm ligands bound terminally to the Ni center. The terminal coordination of the dppm ligand observed rather than binding between the Ni and Al center is relatively unsurprising given the resultant strain of a potential chelate due to the single atom bridge. The Ni center takes on a distorted tetrahedral geometry with respect to the metalloligand phosphine, bound phosphine centers from dppm ligands, and across the Al–H bond. The Ni–H and Al–H distances range from 1.43–1.47(12) Å and 1.55–1.72(12) Å respectively. Notably, the hydride moiety could only be located in two of the four molecules within the asymmetric unit. The distorted tetrahedral geometry about Ni underscores a preference for the Ni-alane designation rather than a Ni-aluminyl. The Ni–Al distances range from 2.269–2.275(4) Å which is a contraction from both **1** and **2-(PPh$_3$)$_2$**. Similar to **2-(PPh$_3$)$_2$**, only one methoxy ligand is bound to the Al center.

Given the consistency in the observation of route C from Scheme 1, perturbing the electron density within the Al–H–Ni subunit by adding ancillary ligands of increasing sigma donation became of greater interest. Thus far, increasingly sigma donating ligands resulted in (1) a Ni–Al contraction in the solid-state and (2) a progressively upfield chemical shift for the hydride moiety. Substitution of more electron rich phosphine ligands to known heterometallic complexes have also demonstrated an impact in accessing challenging reactivity.[51] Addition of two equivalents of trimethylphosphine to LAlH and $Ni(COD)_2$ results in the quantitative formation of **2-(PMe$_3$)$_2$**. The assignment is supported by multinuclear NMR spectroscopy with a doublet and triplet resonance in the $^{31}P\{^1H\}$ NMR spectrum. The triplet at δ −9.18 and doublet at δ −21.11, correspond to the metalloligand phosphorus center and trimethyl phosphine phosphorus centers, respectively. A J_{HP} coupling constant of 9.1 Hz is observed between the two phosphorus environments. The ^1H NMR spectra also support the assignment of the formation of the heterobimetallic **2-(PMe$_3$)$_2$** species. The hydride resonance once again is observed as an apparent broad doublet, the J_{HP} coupling constant is 54.5 Hz. Gratifyingly, the hydride resonance shifts substantially upfield to δ −3.28 in comparison to complexes **1**, **2-(PPh$_3$)$_2$**, and **2-(dppm)$_2$**.

The solid-state structure of **2-(PMe$_3$)$_2$** was also obtained and a significantly shortened Ni–Al interaction is observed (2.261 (1) Å) which is among the shortest Ni–Al distances reported (Fig. 2c).[52] The hydride was located on the electron difference map Ni–H and Al–H distances of 1.61–1.67(4) Å and 1.67–1.71 (4) Å, respectively. Similar to the other complexes discussed in the **2-(L)$_2$** series, a slight distortion of tetrahedral geometry is observed when considering the three phosphine ligands and hydride by the Ni center (τ'_4 = 0.87). Once more, the solid-state structure shows only one of the methoxy ligands remains bound to the Al, again supporting that coordination of the methoxy ligands to the Al center is dependent on the Lewis-acidity of Al.

Synthesis and characterization of an anionic NiAl heterobimetallic hydride complex

The comparative spectral and structural parameters of **1** and **2-(L)$_2$** demonstrate a trend that more sigma donating ligands result in a stronger Ni–Al interaction, as indicated by the bond length contractions. Furthermore, a correlation is also observed relating increasingly upfield hydride chemical shifts with more electron-rich ancillary ligands. Motivated by leaning further on this scale, strongly sigma-donating N-heterocyclic carbene ligands were then employed. Addition of 1,3-diisopropyl-4,5-dimethylimidazol-2-ylidene (iPrMe) to complex **2-(PMe$_3$)$_2$** was investigated to access a carbene coordination complex while minimizing need for metalloligand dissociation. Monitoring the reaction through NMR spectroscopy revealed clean conversion to a single heterometallic species with resonances consistent with incorporation of the N-heterocycle moiety as well as PMe_3 ligands. Remarkably, rather than a carbene coordinated species, an anionic NiAl-

hydride species, complex **3**, is formed. The carbene ligand facilitates demethylation from one of the methoxy groups to form an Al-phenolate and a methylated imidazolium counter cation (Scheme 3). Though carbene ligands have been reported to generate phenolates through demethylation[53] the observed reactivity is somewhat surprising given the presence of the hydride ligands, which one may have expected to be particularly prone to abstraction. The selective formation of complex **3** highlights that the bridged hydride bears a stabilizing role within these frameworks. Furthermore, formation of **3** demonstrates that access to anionic states within catalytic insertion chemistry should be considered and warrants exploration in mechanistic studies. The choice of carbene and heterometallic combination seems to be rather consequential as comparative reactivity of iPrMe with complex **1** produced an indiscernible mixture of complexes *via* NMR spectroscopic studies. Potential rationale is the formation of a mixture of anionic species as well as carbene coordination complexes. The variance in reactivity between **1** and **2-(PMe$_3$)$_3$** towards the carbene ligand is intriguing and could be correlated to an increased dissociative nature of LAlH as opposed to PMe$_3$. Furthermore, addition of bulkier carbene ligand, IPr, to complex **1** shows surprisingly no evidence of reactivity.

Despite the deviation from the ligand substitution reactions, isolation of complex **3** presented a unique opportunity to interrogate the impact of negative charge on the Al–H–Ni subunit. Complex **3** bears only slight solubility in aromatic solvents and thus more polar solvents were employed for characterization. The $^{31}P\{^1H\}$ NMR spectrum in THF-D$_8$ shows that complex **3** is desymmetrized and three resonances are observed at δ −0.65, −16.60, and −25.55 each a doublet of doublets with corresponding coupling constants for *J*-coupling to the neighboring phosphorus centers. The ^1H NMR spectrum is also consistent with the desymmetrized nature of complex **3**, and features resonances for both the anionic NiAl-hydride complex as well as the methylated imidazolium fragment. Intriguingly, the hydride resonance appears at approximately δ −4.07 as a broad apparent doublet and bears a J_{HP} coupling constant of 44.8 Hz, the coupling is better resolved in a crude NMR spectrum in C_6D_6 (Fig. S1–S14†). The chemical shift of the hydride resonance in complex **3** presents the most upfield of the Al–H–Ni series within the study.

The solid-state structure of complex **3** was obtained and confirmed the assignment of the anionic nickel–aluminum species and a methylated imidazolium cation (Fig. 3). The anion in complex **3** can be described within the extremes as

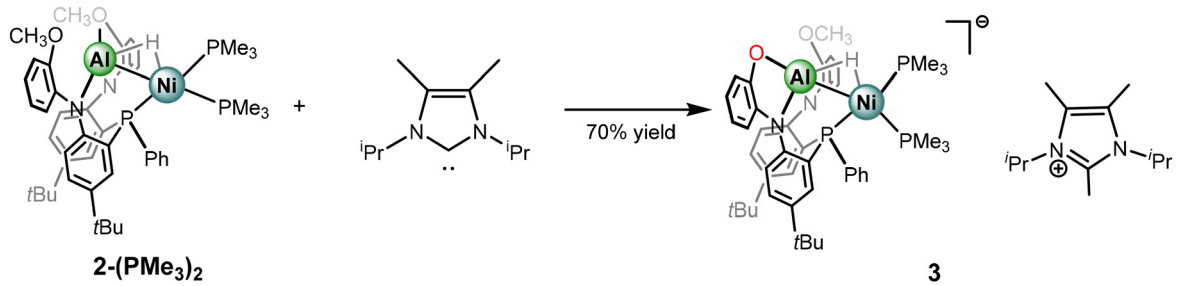

Scheme 3 Synthesis of anionic NiAl hydride complex **3**.

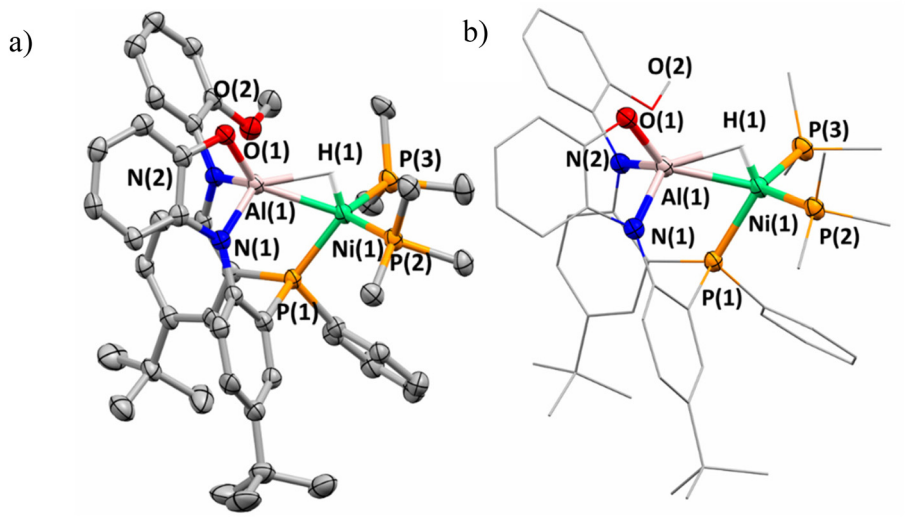

Fig. 3 (a) Solid-state structure of anionic portion of complex **3**. Cation and hydrogen atoms on ligands are excluded for clarity. (b) Mixed wire-frame/ellipsoid structure of complex **3** shown for clarity.

either a nickel aluminate or a nickelate-alane given the literature precedent for accessing both aluminate[54] and nickelate complexes in heterometallic species.[55,56] Both the solid-state structure of complex **3** and the chemical shift support the retention of the hydride moiety in a bridged nature. The Ni–Al distance of 2.333(1) Å demonstrates that complex **3** undergoes an elongation in comparison to **2-(PMe$_3$)$_2$**. Despite the Ni–Al distance elongation in complex **3**, the complexes within this study feature a Ni–Al bond distance that are less than the sum of the covalent radii of Ni and Al.[57] Complex **3** establishes the only observation where the chemical shift of the hydride moiety continues to trend upfield while a elongation of the Ni–Al interaction is observed (Fig. 4). A table comparing the solid-state structural patterns of complexes **1**, **2-(L)$_2$**, and **3** is shown in Table 1. Complex **3** demonstrates a mild distortion from tetrahedral geometry at Ni with respect to the hydride moiety and three phosphine centers with the largest distortion amongst the class of molecules (τ'_4 = 0.80).

Electronic structure studies

The study of the series of NiAl-hydride complexes reveals an intriguing trend, the inclusion of more electron rich ancillary ligands, as well as negative charge, results in increasingly upfield chemical shifts of the hydride moieties. The principles

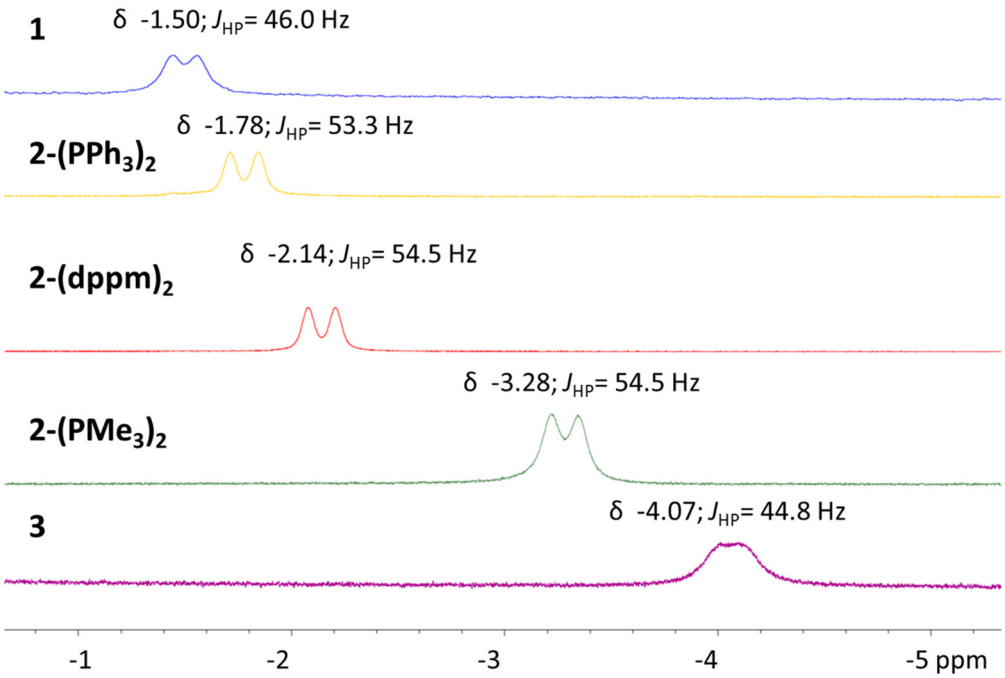

Fig. 4 Stacked ^{1}H NMR spectra in hydride region for complexes **1**, **2-(L)$_2$**, and **3**.

Table 1 Comparison of structural and spectroscopic parameters for complexes **1**, **2(L)$_2$**, and **3**

	1	**2-(PPh$_3$)$_2$**	**2-(dppm)$_2$**	**2-(PMe$_3$)$_2$**	**3**
Ni–Al (Å)	2.3629(7) 2.3683(7)	2.3222(16)	2.269–2.276(4)	2.2503(7) 2.2613(7)	2.3336(11) 2.3358(11)
Ni–H (Å)	1.57(3) 1.60(3)	1.54(4)	1.43–1.47(13)	1.61(4) 1.67(4)	1.19(3) 1.31(3)
Al–H (Å)	1.59(3) 1.61(3)	1.74(4)	1.55–1.72(12)	1.68(4) 1.71(4)	1.88(3) 1.75(3)
Ni–P(1) (Å)	2.1580(6) 2.1635(6)	2.1832(14)	2.169–2.175(2)	2.1410(6) 2.1449(6)	2.1311(10) 2.1329(10)
Ni–(P2/P3) (Å)	—	2.2095(14) 2.1915(16)	2.171–2.186(2)	2.1570(7) 2.1612(7) 2.1674(7) 2.1706(7)	2.1661(11) 2.1614(11) 2.1559(11) 2.1677(10)
Ni τ'_4	0.89(0.86)[a]	0.92(0.87)	0.90(0.86)	0.87(0.84)	0.80(0.82)
Al τ'_4	0.23(0.37)[b]	0.76(0.80)	0.73(0.72)	0.70(0.69)	0.78(0.80)
δ Al–H–Ni	−1.50	−1.78	−2.14	−3.28	−4.07

[a] Values in brackets determined from DFT-optimized structures. [b] τ_5 value.

that govern chemical shift are non-trivial and convoluted;[58] however, diamagnetic Ni-hydrides often have chemical shifts in the range of −5 to −38 ppm, (with the majority not lying within the extremes)[59] while diamagnetic aluminum hydride species have chemical shifts typically ranging from 3–6 ppm.[60–62] The chemical shifts of the complexes reported here show an intermediary of the two, consistent with a designation of sigma-complexes.[59] Moreover, comparison of the Tolman parameters of similar ancillary ligands[63,64] employed in the **2-(L)$_2$** series are in agreement with the upfield chemical shifts belonging to more donating ligands; though, this comparison excludes complex **1** and complex **3**.

The described trend could be explained by consideration of the 3-center bonding motif within the Al–H–Ni subunit. One could argue that predominant interactions within the subunit are donation of electron density from an Al–H sigma-bonding orbital to the Ni center and backdonation from the Ni center to the Al–H sigma antibonding orbital, as described in the introduction. Notably, more electron rich Ni centers would be best suited for a strengthened back donation interaction. Within the series of complexes discussed here, the strength of the backbonding interaction would delineate the degree of Ni–H character observed, akin to arguments for dihydrogen coordinated intermediates prior to formation of metal-dihydrides.[65] Similar arguments for Mg-hydrides and Zn-hydrides to Pd centers have been depicted previously.[34] However, unlike the prototypical dihydrogen coordination, the interaction is asymmetric; where the accepting orbital from the main group-hydride is of greater main group-element character. Consequently, donation and backdonation interactions are likely not evenly distributed. Physical methods to quantify the electron distribution within an Al–H–Ni subunit are not well developed, mostly due to the lack of known examples. Although Al is spin active, the quadrupolar nature limits the insight one can glean from Al–H coupling constants, compared to those of silane-coordinated sigma species.[66] In this series of complexes, the only observable coupling constant for the hydrides is to the metalloligand phosphine center as confirmed through $^{1}H\{^{31}P\}$ NMR experiments.[40] Nevertheless, the chemical shift of the hydride moiety trends progressively upfield across the series (Fig. 4). A finding consistent with a gradual shift towards Ni–H character across the continuum of bonding within the subunit.

The structure across the series of complexes was evaluated for changes at both Al and the Ni centers. As discussed above, the expectation for a Ni-alane would result in a tetrahedral geometry while the Ni-aluminyl would likely adapt a square planar geometry. Thus, the evaluation of the τ'_4 value at Ni across the series serves as an informative metric to guide the level of deviation from tetrahedral Ni-alane. Indeed, analysis of τ'_4 across the series of complexes reported here show an increasing deviation from **1** (perfectly tetrahedral) across the series of heterobimetallic complexes examined, ranging from 0.92 to 0.80, consistent with the trend in chemical shift of the hydride ligand, a finding again supporting a gradual shift to more Ni–H character (Table 1). Given the major structural differences and bidentate nature in metalloligand LAlH in comparison to the phosphine donors examined, it is not surprising heterotrimetallic complex **1** slightly deviates from the trend. Comparison of τ values is more complicated at Al given the increased coordination number at complex **1**. Across the heterobimetallic complexes there seems to be a consistent deviation from tetrahedral geometry with exception to complex **3**. This deviation is potentially associated to the anionic nature and the overall structural difference that a phenolate moiety would impose rather than an aryl ether. Given that both τ'_4 values at Ni and Al utilize bond angles determined from the hydride location, the τ'_4 value was also calculated from the DFT-optimized structures (discussed below); the results show strong consistency with the trends discussed above.

To deepen our understanding within this argument, density functional theory (DFT) and Quantum Theory Atoms-In-Molecules (QTAIM) calculations were performed to interrogate the electronic structure, while also gaining more reliable metrics regarding the metal hydride bond lengths. The bond lengths from DFT-optimized structures correlate well with experimental results (Table S3-1†) with exception to metal–hydride bond lengths in **2-(dppm)$_2$**, **2-(PPh$_3$)$_2$** and **3**; in these cases the DFT-calculated structure is deemed a better representation of the hydride position given challenges in predicting hydride locations accurately through X-ray diffraction. Representative examples highlighting interactions within the core are observed in the HOMO and HOMO−6 of **2-(PMe$_3$)$_2$** (Fig. 5). The HOMO of **2-(PMe$_3$)$_2$** specifically demonstrates contributions from all three components of the subunit; Ni (64%), Al (3.6%), and H (6.4%). The primary contributors from Al are the 3s (2.03%) and 2p$_y$ (0.99%) orbitals, while the Ni orbital contributors are a hybrid mixture mostly consistent with 3d (~55.3%) with some 4p (~9%) character. Orbital mixing into the ligand framework renders further evaluation difficult to deconvolute; however, the frontier orbitals demonstrate significant contributions from the Ni centers across the series of complexes, their details of which are displayed upon in Tables S3-3 to S3-7.†

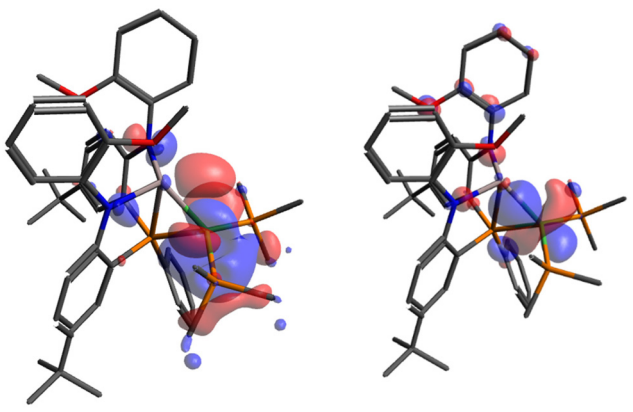

Fig. 5 Pictorial representation of HOMO (left) and HOMO (−6) (right) of **2-(PMe$_3$)$_2$**. Isosurface value set to 0.03 e A^{-3}. Hydrogen atoms are omitted for clarity.

Table 2 Comparison of key bond lengths, Wiberg Bond Indices (WBI) from DFT-optimized structures and ρ values from QTAIM calculations

Metric		1	2-$(PPh_3)_2$	2-$(dppm)_2$	2-$(PMe_3)_2$	3
Key bond lengths of DFT optimized structures (Å)	Ni–Al	2.321, 2.341	2.264	2.278	2.254	2.343
	Ni–H	1.627, 1.659	1.636	1.637	1.658	1.621
	Al–H	1.700, 1.707	1.713	1.730	1.727	1.734
Wiberg bond indices	Ni–Al	0.30, 0.31	0.35	0.36	0.39	0.34
	Ni–H	0.47, 0.48	0.48	0.49	0.49	0.52
	Al–H	0.36, 0.39	0.37	0.37	0.40	0.37
$\rho(r)$ (electron density at bond critical points)	Ni–Al	—	—	—	—	—
	Ni–H	0.09	0.09	0.09	0.09	0.09
	Al–H	0.07	0.06	0.06	0.07	0.06

Table 2 summarizes key metrical bonding parameters within the Al–H–Ni subunits of complexes **1**, **2-$(L)_2$**, and **3** including the computationally determined bond lengths, Wiberg Bond Indices (WBI), and QTAIM (3, −1) critical points. The bond orders of Ni–Al, Ni–H and Al–H are all relatively close and range between 0.30 and 0.52, the values themselves are consistent with known heterometallic hydride complexes and provide more support for the classification of a 3-center bonding motif within the series of complexes.[34] Examining the WBI values across the series of complexes with varying ancillary ligands demonstrate moderate changes and are generally in agreement that the stronger sigma-donating ancillary ligands leads to an increase in the Ni–Al bonding interaction. Furthermore, the decrease in the Ni–Al WBI for complex **3** is consistent with the longer bond length in both the crystallographically determined and the DFT-optimized structures. Studies probing metal–metal interactions with Rh and varying metals have shown similar consistency with an increased WBI value correlated to a shorter crystallographically determined Rh–M bond.[67] Despite the diminished Ni–Al bonding interaction in **3**, an increase for the Ni–H WBI is observed, and in agreement with a trend correlating slight increases in the Ni–H WBI to increasingly upfield hydride chemical shifts. The computational studies were further buttressed with Quantum Theory of Atoms-In-Molecules (QTAIM) analysis to identify the (3, −1) bond critical points (BCPs) within the Al–H–Ni subunit (Table S3-2†).[68,69] Gratifyingly, BCPs with $\rho(r)$ values ranging from 0.06 to 0.09 were observed between Al–H and Ni–H bonds substantiating the 3-center bonding motif.[20] Critical points were not identified between Ni and Al centers; consistent with known TaCu-hydride complexes with strong metal–metal interactions.[70]

Intriguingly, the difference in NPA charges with Ni and Al suggest strong polarization between the two metal centers (Table S3-2†). The high negative charge at Ni, specifically, is consistent with reported examples describing partial anionic character at the transition metal center,[26,71–73] and contrasts the slightly positive values, at Ni, of heterometallic Ni–H–Mg complexes. Crucially, the NPA charge distribution data should be interpreted with caution as NPA charges have been shown to overestimate negative charge in heterometallic systems.[74] QTAIM derived charges decrease substantially in comparison to the NPA-derived charges; a finding analogous to reported FeAl and FeCu complexes.[74]

Early reports studying late metal hydrides and phosphine ancillary ligands outline that altering the electron rich nature of the phosphine centers influenced the hydricity of the moiety and is presented through an upfield chemical shift.[75,76] The hydricity amongst the heterometallic series of complexes were evaluated through DFT calculations with solvation in acetonitrile.[77] Generally, more electron rich phosphine donors were found to lead to a more hydridic hydride ligand (Table S3-8†); consistent with literature examples of nickel bisphosphine systems.[78,79] For example, complex **2-$(PPh_3)_2$** features a ΔG°_H of 59.3 kcal mol^{-1} which is considered moderate amongst neutral Ni species; however, **2-$(PMe_3)_2$** demonstrates a heightened hydricity (ΔG°_H of 54.1 kcal mol^{-1}). Amongst the series of complexes, **3** proved to be the strongest hydride donor by far $\left(\Delta G^\circ_H = 40.1\,\text{kcal mol}^{-1}\right)$, which the anionic charge of the system is likely accountable for.[80] Further studies to correlate hydricity in separate reactivity studies are underway. Lastly, IR spectroscopy was examined to interrogate the impact that the sigma donating ability of the ligands bear on the metal-hydride stretches (Fig. S5-1 to S5-5†). The bridging nature of the hydrides likely result in broadening of the metal-hydride stretches. However, DFT calculations indicate a gradual decrease in the M–H wavenumber for ligands with stronger donating ability among the neutral heterometallics (Table S5-1†).

Conclusions

With the aim of gaining a thorough understanding of the nature of the hydride moiety in **1**, a series of complexes were synthesized and characterized that feature an Al–H–Ni subunit. The series of complexes discussed above demonstrate the relative ease of synthetic access to sigma complexes of alanes to Ni centers, as well as the surprising stability of the resultant Al–H–Ni subunits. The observation of metalloligand dissociation in cases where phosphine ancillary ligands were introduced underscores that full hydride migration to either metal center has, thus far, not been accessible while maintaining the core trimetallic structure in **1**. Nevertheless, key insights were garnered through examining the impact of the coordinated ancillary ligands towards the remaining Al–H–Ni subunits in the **2-$(L)_2$** complexes. Namely, the introduction of increasingly strong

sigma donating phosphine ligands perturb the electron distribution within the Al–H–Ni subunit of the neutral heterometallic species, which is evidenced by progressively contracted Ni–Al bond distances as well as more upfield chemical shifts for the hydride moieties. Furthermore, the Al–H–Ni subunit proved to persist despite changes in the charge of the molecule as imposed in anionic complex **3**. Complexes **1** and **2-(L)$_2$** abide by the principles described in the sigma-bonding continuum (Fig. 1; bottom) relating the shortening of a Ni–Al distance with more Ni–H character. Conversely, complex **3**, which according to spectroscopic and computational studies bears the most Ni–H character in the series, forces a deviation from the accepted trend.

Computational studies support the 3-center bonding nature of the Al–H–Ni subunit and outline mild changes across the series but a general agreement in the correlation of strength of the sigma-donor leading to an increased Ni–Al interaction. Cumulatively, crystallographic, spectroscopic, and computational studies support that, with respect to the discussed bonding continuum, the hydride moiety shifts slightly towards more Ni–H character and becomes increasingly hydridic with more electron donating ancillary ligands as well as the introduction of negative charge to the framework. Although option **C**, from Scheme 1, is the dominant pathway observed in this study, ongoing efforts in accessing options **A** and **B** are underway. Additional studies are focused on examining the impact of varying ancillary ligands in insertion chemistry and identifying methodology to spectroscopically determine the nature of the hydride moieties in Al–H–Ni systems.

Experimental

General procedures

All air- and water-sensitive compounds were manipulated under N_2 using standard Schlenk or glovebox techniques. The solvents for air- and moisture-sensitive reactions were dried over activated 3 Å molecular sieves and the anhydrous nature was confirmed by addition of persistence of ketyl radical upon addition. Deuterated solvents were purchased from Millipore Sigma; C_6D_6, and C_7D_8 was dried as mentioned above. Potassium was purchased from Millipore Sigma and used without further purification. 1,3-Diisopropylthiourea, 3-hydroxy-2-butanone, and 1-hexanol, triphenylphosphine, trimethylphosphine, and bis-diphenylphosphinomethane were purchased from Oakwood Chemical and Millipore Sigma and used without further purification once purity was confirmed by NMR spectroscopy. 1,3-Bis(isopropyl)-4,5(dimethyl)imidazol-2-ylidene[81] and **1**[40] were synthesized according to the literature procedure. All ^{1}H, ^{13}C, and ^{31}P spectra of organic and organometallic compounds were recorded on a Bruker 400 MHz spectrometer. ^{1}H and ^{13}C chemical shifts are reported relative to residual solvent resonances. ^{31}P{^{1}H} NMR spectra were referenced to external 85% H_3PO_4 at δ 0.00. IR spectroscopy was carried out on a Thermo Scientific Nicolet iS5 FTIR spectrometer.

Synthesis of complex 2-(PPh$_3$)$_2$

Method A: in a N_2 filled glovebox, a solution of **1** (20.0 mg, 0.015 mmol) in 0.6 mL of C_6D_6 in a 20 mL scintillation vial was added four equivalents of triphenyl phosphine (16.3 mg, 0.060 mmol) and an equivalent of Ni(COD)$_2$ (4.1 mg, 0.015 mmol) simultaneously. Over the course of an hour, the solution turned dark orange and multinuclear NMR indicated the quantitative formation of complex **2-(PPh$_3$)$_2$**. The volatiles of the reaction mixture were removed and triturated with *n*-pentane (3 × 1 mL). The crude orange solid was washed with *n*-pentane (1 mL) and diethyl ether (1 mL) and then extracted with benzene and filtered through a pad of Celite. The bright orange solution was evaporated yielding analytically pure **2-(PPh$_3$)$_2$** (31.8 mg, 0.026 mmol) in 86.7% yield. **Method B**: to a solution of LAlH (500 mg, 0.78 mmol) in 10 mL of benzene in a 50 mL round bottom flask was added one equivalent of Ni(COD)$_2$ (215 mg, 0.78 mmol) and two equivalents of triphenylphosphine (409 mg, 1.56 mmol) simultaneously resulting in the formation of a dark yellow solution. The solution was stirred for 0.25 hours at which point all volatiles were removed *in vacuo*. The dark yellow crude mixture was triturated with *n*-pentane (3 × 5 mL) and then washed with pentane (10 mL) and diethyl ether (10 mL) and then extracted with benzene (12 mL) and filtered through a Celite pad in the filter frit. The benzene solution of **2-(PPh$_3$)$_2$** was evaporated resulting in analytically pure **2-(PPh$_3$)$_2$** (410.0 mg, 0.36 mmol) in 46% yield. Single-crystal X-ray quality crystals were grown by vapor diffusion of *n*-pentane to a concentrated solution of **2-(PPh$_3$)$_2$** in benzene. ^{1}H NMR (400 MHz, C_6D_6, 298 K): δ 7.57 (d, $^3J_{HH}$ = 9.4 Hz, 2H, PhH), 7.36 (t, $^3J_{HH}$ = 8.0 Hz, 12H, PhH), 7.24 (broad m, $W_{1/2}$ = 14.4 Hz, 2H, PhH), 6.94–6.88 (overlapping m, 21H, PhH), 6.69 (broad m, $W_{1/2}$ = 12.4 Hz, 4H, PhH), 6.49 (apparent t, $^3J_{HH}$ = 8.1 Hz, 2H, PhH), 6.32 (broad multiplet, $W_{1/2}$ = 12.3 Hz, 2H, PhH), 2.96 (s, 6H, OCH_3), 1.15 (s, 18H, $C(CH_3)_3$), −1.78 (apparent d, J_{HP} = 53.3 Hz, 1H, Al–H–Ni). ^{31}P{^{1}H} NMR (242.87 MHz, C_6D_6, 298 K): δ 29.26 (broad s, $W_{1/2}$ = 40.3 Hz, 2P, PPh_3), −12.48 (t, $^2J_{PP}$ = 11.2 Hz, 1P, PPhAr). ^{31}P{^{1}H} NMR (242.87 MHz, C_7D_8, 328 K): δ 29.01 (d, $^2J_{PP}$ = 9.6 Hz, 2P, PPh_3), −12.40 (t, $^2J_{PP}$ = 9.6 Hz, 1P, PPhAr). ^{13}C{^{1}H} NMR (101 MHz, C_6D_6, 298 K): δ 151.9 (overlapping m, aryl-C), 140.34 (2nd order multiplet, AXX′Y, aryl-C), 137.58 (d, J_{CP} = 5.4 Hz, aryl-C), 137.47 (s, aryl-C), 136.51 (dt, $^1J_{CP}$ = 37.6 Hz, J_{CP} = 3.5 Hz, aryl-C), 133.71 (2nd order multiplet, AXX′Y, aryl-C), 133.09 (d, J_{CP} = 11.1 Hz, aryl-C), 129.54 (broad s, $W_{1/2}$ = 15.4 Hz, aryl-C), 128.23 (s, aryl-C), 127.28 (overlapping m, aryl-C), 126.95 (d, J_{CP} = 8.4 Hz, aryl-C), 126.13 (s, aryl-C), 125.39 (s, aryl C), 123.57 (broad s, $W_{1/2}$ = 24.8 Hz, aryl-C), 122.40 (s, aryl-C), 120.69 (broad s, $W_{1/2}$ = 181.5 Hz, aryl-C), 120.25 (s, aryl-C), 115.20 (s, J_{CP} = 5.8 Hz, aryl-C), 109.46 (s, aryl-C), 55.07 (s, OCH_3), 33.85 (s, $C(CH_3)_3$), 31.31 (s, $C(CH_3)_3$). $C_{76}H_{74}AlN_2NiO_2P_3$ theoretical: C% 74.45, H% 6.08, N% 2.28. Determined C% 74.48, H% 6.28, N% 2.04.

Synthesis of complex 2-(dppm)$_2$

To a solution of LAlH (450.0 mg, 0.70 mmol) in 4 mL in benzene was added bis-diphenylphosphinemethane (478.3 mg, 1.24 mmol) followed by addition of a solution of Ni(COD)$_2$ (171.1 mg, 0.62 mmol) in 4 mL of benzene. Over the course of four hours, the color of the solution changed from yellow to mahogany. All volatiles were removed *in vacuo* and the crude mixture was triturated with *n*-pentane (3 × 4 mL) and then washed with pentane (10 mL) and diethyl ether (7 mL) and then extracted with benzene (5 mL). The benzene fraction was evaporated resulting in analytically pure **2-(dppm)$_2$** in 41.4% yield (379.0 mg, 0.26 mmol). Crystals of sufficient quality for single-crystal X-diffraction were grown from benzene/HMDSO slow evaporation. ^{1}H NMR (400 MHz, C_6D_6, 298 K): δ 7.62 (d, $^3J_{HH}$ = 8.4 Hz, 2H, PhH), 7.53 (d, $^3J_{HH}$ = 10.0 Hz, 2H, PhH), 7.29–6.65 (overlapping m, PhH), 6.45 (t, $^3J_{HH}$ = 8.5 Hz, 2H, PhH), 6.37 (d, $^3J_{HH}$ = 7.8 Hz, 2H, PhH), 3.17 (dd, $^2J_{HP}$ = 41.5 Hz, $^2J_{HP}$ = 14.5 Hz, 4H, PCH_2P), 3.09 (s, 6H, OCH_3), 1.15 (s, 18H, $C(CH_3)_3$), −2.14 (apparent d, J_{HP} = 54.5 Hz, $W_{1/2}$ = 80.6 Hz, 2H, Al–H–Ni). ^{31}P{^{1}H} NMR (242.87 MHz, C_6D_6, 298 K): δ 20.75 (broad s, $W_{1/2}$ = 115.3 Hz, 2P, M-*P*$Ph_2CH_2PPh_2$), −12.36 (t, $^2J_{PP}$ = 12.0 Hz, 1P, PPhAr), −27.06 (apparent d, $^2J_{PP}$ = 41.0 Hz, 2P, M-PPh_2CH_2*P*Ph_2). ^{31}P{^{1}H} NMR (242.87 MHz, C_7D_8, 253 K): δ 26.78 (broad m, $W_{1/2}$ = 395.3 Hz, 1P, M-*P*$Ph_2CH_2PPh_2$), 15.46 (broad m, $W_{1/2}$ = 395.3 Hz, 1P, M-*P*$Ph_2CH_2PPh_2$), −12.50 (t, $^2J_{PP}$ = 11.0 Hz, 1P, PPhAr), −25.92 (broad m, $W_{1/2}$ = 395.3 Hz, 1P, M-PPh_2CH_2*P*Ph_2), −29.40 (broad m, $W_{1/2}$ = 395.3 Hz, 1P, M-PPh_2CH_2*P*Ph_2). ^{31}P{^{1}H} NMR (242.87 MHz, C_7D_8, 333 K): δ 20.98 (2nd order multiplet, AA′XX′Y, 2P, M-*P*$Ph_2CH_2PPh_2$), −11.46 (t, $^2J_{PP}$ = 11.0 Hz, 1P, PPhAr), −27.06 (2nd order multiplet, AA′XX′Y, 2P, M-PPh_2CH_2*P*Ph_2). ^{13}C{^{1}H} NMR (101 MHz, C_6D_6, 298 K): δ 152.17 (overlapping broad m, aryl-C), 141.24 (2nd order multiplet, aryl-C), 139.36 (2nd order multiplet, aryl-C), 138.54 (broad m, aryl-C), 137.81 (s, aryl-C), 137.53 (broad m, $W_{1/2}$ = 13.4 Hz, aryl-C), 137.02 (dt, J_{CP} = 38.2 Hz, J_{CP} = 4.7 Hz, aryl-C), 133.24 (broad d, J_{CP} = 11.7 Hz, aryl-C), 132.82 (dd, J_{CP} = 20.2 Hz, J_{CP} = 7.7 Hz, aryl-C), 132.65 (doublet of m, J_{CP} = 98.2 Hz, aryl-C), 132.47 (d, J_{CP} = 12.7 Hz, aryl-C), 129.58 (broad m, $W_{1/2}$ = 19.6 Hz, aryl-C), 128.23 (s, aryl-C), 127.35–127.09 (overlapping m, aryl-C), 126.95 (d, J_{CP} = 8.7 Hz, aryl-C), 125.93 (s, aryl-C), 125.41 (s, aryl-C), 123.53 (broad s, $W_{1/2}$ = 64.4 Hz, aryl-C), 122.50 (s, aryl-C), 120.19 (broad s, $W_{1/2}$ = 63.5 Hz, aryl-C), 115.30 (d, J_{CP} = 5.6 Hz, aryl-C), 109.39 (s, aryl-C), 55.21 (s, OCH_3), 33.31 (s, *C*$(CH_3)_3$), 32.86 (2nd order multiplet AXX′YZ, Ni–Ph_2P–*C*H_2–PPh_2), 31.30 (s, $C(CH_3)_3$). $C_{91}H_{91}AlN_2NiO_2P_5$ theoretical: C% 73.59, H% 6.18, N% 1.82. Determined C% 73.25, H% 6.27, N% 1.97.

Synthesis of complex 2-(PMe$_3$)$_2$

To a solution of LAlH (700.0 mg, 1.088 mmol) in 7 mL in toluene was added a solution of Ni(COD)$_2$ (214 mg, 0.77 mmol) and 1.55 mL of 1.0 M trimethylphosphine solution (1.55 mmol) in 3 mL of toluene, resulting in the formation of a dark brown solution. The solution was stirred for 48 hours at which point all volatiles were removed *in vacuo*. The dark brown crude mixture was triturated with *n*-pentane (3 × 5 mL) and washed thoroughly with pentane (15 mL), diethyl ether (10 mL) and then extracted with benzene (10 mL). The benzene fraction was evaporated resulting in the isolation of an analytically pure bright orange powder (291.0 mg, 0.341 mmol) in 44% yield. The powder is then dissolved in a 50 : 50 mixture of *n*-pentane and diethyl ether and recrystallized at −40 °C to afford X-ray quality bright yellow single crystals of complex **2-(PMe$_3$)$_2$**. ^{1}H NMR (400 MHz, C_6D_6, 298 K): δ 7.91 (apparent t, $^3J_{HH}$ = 8.9 Hz, 4H, PhH), 7.32(d, $^3J_{HH}$ = 8.0 Hz, 2H, PhH), 7.20 (apparent t, $^3J_{HH}$ = 8.0 Hz, 2H, PhH), 7.02–7.14 (overlapping multiplets, 5H, PhH), 6.77 (apparent t, $^3J_{HH}$ = 7.4 Hz, 2H, PhH), 6.69 (apparent t, $^3J_{HH}$ = 7.4 Hz, 2H, PhH), 6.36 (d, $^3J_{HH}$ = 7.9 Hz, 2H, PhH), 3.07 (s, 6H, OCH_3), 1.23 (s, 18H, $C(CH_3)_3$), 0.96 (s, 18H, $P(CH_3)_3$), −3.28 (apparent d, J_{HP} = 54.5 Hz, $W_{1/2}$ = 93.6 Hz, 1H, Al–H–Ni). ^{31}P{^{1}H} NMR (242.87 MHz, C_6D_6, 298 K): δ −9.18 (t, $^2J_{PP}$ = 9.1 Hz, 1P, PPhAr), 21.11 (d, $^2J_{PP}$ = 9.1 Hz, 2P, PMe_3). ^{13}C{^{1}H} NMR (101 MHz, C_6D_6, 298 K): δ 152.41 (d, $^2J_{CP}$ = 14.5 Hz, aryl-C), 152.00 (s, aryl-C), 139.60 (dt, $^1J_{CP}$ = 36.3 Hz, $^2J_{CP}$ = 5.6 Hz, aryl-C), 138.37 (broad s, aryl-C), 137.44 (d, $^2J_{CP}$ = 5.3 Hz, aryl-C), 132.46 (d, $^2J_{CP}$ = 11.6 Hz, aryl-C), 129.08 (s, aryl-C), 126.91 (d, $^2J_{CP}$ = 8.5 Hz, aryl-C), 126.42 (s, aryl-C), 125.43 (s, aryl-C), 123.03 (broad s, aryl-C), 122.55 (broad s, aryl-C), 121.70 (dt, $^1J_{CP}$ = 44.1 Hz, $^2J_{CP}$ = 9.1 Hz, aryl-C), 119.60 (s, aryl-C), 115.69 (d, $^2J_{CP}$ = 6.0 Hz, aryl-C), 110.16 (s, aryl-C), 55.21 (s, OCH_3), 33.86 (s, $C(CH_3)_3$), 31.38 (s, $C(CH_3)_3$), 21.91 (td, $^1J_{CP}$ = 11.1 Hz, $^2J_{CP}$ = 4.5 Hz, $P(CH_3)_3$). $C_{46}H_{62}AlN_2NiO_2P_3$. Theoretical: C% 64.73, H% 7.32, N% 3.28. Determined C% 64.82, H% 7.42, N% 2.97.

Synthesis of complex 3

To a solution of **2-(PMe$_3$)$_2$** (200.0 mg, 0.24 mmol) in 4 mL in benzene was added one equivalent of 1,3-diisopropyl-4,5-dimethylimidazol-2-ylidene (42.7 mg, 0.24 mmol) as a solution in benzene (4 mL) at room temperature. Over the course of one hour, the solution darkened and a yellow precipitate formed. The suspension was transferred to a pipette filter with Celite and the solid precipitate was washed with diethyl ether (5 mL) and the precipitate was then extracted with 10 mL of tetrahydrofuran. The THF solution was then evaporated to yield 69.8% of analytically pure complex **3** (169.1 mg, 0.16 mmol). X-ray quality crystals were grown *via* vapor diffusion of hexamethyldisiloxane to a solution of **3** in THF. ^{1}H NMR (400 MHz, C_4D_8O, 298 K): δ 7.72–7.64 (overlapping m, 3H, PhH), 7.54 (dd, $^3J_{HH}$ = 6.1 Hz, $^3J_{HH}$ = 8.2 Hz, 1H, PhH), 7.36 (apparent t, $^3J_{HH}$ = 6.2 Hz, 1H, PhH), 7.22 (apparent t, $^3J_{HH}$ = 7.2 Hz, 2H, PhH), 7.14 (apparent t, $^3J_{HH}$ = 7.2 Hz, 1H, PhH), 7.05 (d, $^3J_{HH}$ = 7.1 Hz, 1H, PhH), 6.95 (apparent t, $^3J_{HH}$ = 10.7 Hz, 2H, PhH), 6.82 (apparent t, $^3J_{HH}$ = 7.5 Hz, 1H, PhH), 6.77–6.63 (overlapping multiplets, 3H, PhH), 6.43 (d, $^3J_{HH}$ = 7.2 Hz, 2H, PhH), 6.30 (t, $^3J_{HH}$ = 7.3 Hz, 1H, PhH), 6.06 (apparent t, $^3J_{HH}$ = 7.2 Hz, 1H, PhH), 5.99 (apparent t, $^3J_{HH}$ = 7.2 Hz, 1H, PhH), 4.37 (sep, $^3J_{HH}$ = 7.2 Hz, 2H, C*H*$(CH_3)_2$), 3.48 (s, 3H, OCH_3), 2.06 (overlapping s, 9H, imidazolium CH_3), 1.25 (d,

$^{3}J_{HH}$ = 7.2 Hz, 12H, CH(CH_3)$_2$), 1.23 (s, 9H, C(CH_3)$_3$), 1.10 (s, 9H, C(CH_3)$_3$), 0.85 (d, $^{3}J_{HH}$ = 4.2 Hz, 9H), 0.72 (d, $^{3}J_{HH}$ = 4.2 Hz, 9H), −4.07 (apparent d, J_{HP} = 44.8 Hz, $W_{1/2}$ = 115.2 Hz, 1H, Al–H–Ni). ^{31}P{^{1}H} NMR (242.87 MHz, C_4D_8O, 298 K): δ −0.65 (dd, $^{2}J_{PP}$ = 32.5 Hz, $^{2}J_{PP}$ = 6.4 Hz, 1P, PPhAr), −16.60, (dd, $^{2}J_{PP}$ = 30.5 Hz, $^{2}J_{PP}$ = 6.4 Hz, 1P, P(CH_3)$_3$), −25.45 (dd, $^{2}J_{PP}$ = 30.5 Hz, $^{2}J_{PP}$ = 32.5 Hz, 1P, P(CH_3)$_3$). ^{13}C{^{1}H} NMR (101 MHz, C_4D_8O, 298 K): δ 158.06 (s, aryl-C), 157.90 (d, J_{CP} = 17.5 Hz, aryl-C), 156.07 (s, aryl-C), 150.53 (d, J_{CP} = 12.0 Hz, aryl-C), 143.21 (ddd, J_{CP} = 26.4 Hz, J_{CP} = 10.9 Hz, J_{CP} = 1.8 Hz, aryl-C), 142.07 (s, aryl-C), 141.76 (s, aryl-C), 139.13 (s, aryl-C), 134.74 (d, J_{CP} = 5.5 Hz, aryl-C), 132.80 (d, J_{CP} = 12.4 Hz, aryl-C), 132.36 (d, J_{CP} = 4.6 Hz, aryl-C), 132.18 (s, aryl-C), 130.33 (s, ary-C), 127.48 (ddd, J_{CP} = 42.9 Hz, J_{CP} = 13.3 Hz, J_{CP} = 8.5 Hz, aryl-C), 125.95 (d, J_{CP} = 8.8 Hz, aryl-C), 125.66 (s, aryl-C), 125.05 (s, aryl-C), 124.66 (s, aryl-C), 124.24 (s, aryl-C), 121.99 (s, aryl-C), 120.95 (s, aryl-C), 119.92 (s, aryl-C), 116.45 (dd, J_{CP} = 19.0 Hz, J_{CP} = 17.5 Hz, aryl-C), 116.16 (d, J_{CP} = 6.3 Hz, aryl-C), 116.08 (s, aryl-C), 113.66 (s, aryl-C), 113.41 (d, J_{CP} = 5.6 Hz, aryl-C), 113.24 (s, aryl-C), 112.41 (s, aryl-C), 111.16 (s, aryl-C), 54.44 (s, CH(CH$_3$)$_2$), 50.38 (s, OCH$_3$), 33.69 (s, C(CH$_3$)$_3$), 33.35 (s, C(CH$_3$)$_3$), 31.37 (s, C(CH$_3$)$_3$), 31.11 (s, C(CH$_3$)$_3$), 22.50 (ddd, J_{CP} = 12.6 Hz, J_{CP} = 7.4 Hz, J_{CP} = 5.2 Hz, P(CH$_3$)$_3$), 21.69 (ddd, J_{CP} = 13.2 Hz, J_{CP} = 7.8 Hz, J_{CP} = 5.5 Hz, P(CH$_3$)$_3$), 20.27 (s, CH(CH$_3$)$_2$), 10.24 (s, ^{i}PrNCCH$_3$), 8.84 (s, NCCH$_3$CCH$_3$N). $C_{57}H_{82}AlN_4NiO_2P_3$ theoretical: C% 66.22, H% 7.99, N% 5.42. Determined C% 66.20, H% 7.99, N% 5.23.

Computational details

The initial starting point geometries were adapted from the corresponding crystallographically obtained structures and optimized to a stationary point, followed by analytical frequency calculations to confirm that no imaginary frequencies were present. Geometry optimization was performed for all the complexes using the BP86 density functional.[82,83] A mixed basis set scheme was employed, in which H, C, N, O and P were described by the def2-SVP basis set[84] while Al and Ni were described by the larger def2-TZVP basis set.[85] Vibrational analysis was then performed on the same level to verify that all the optimized structures are true stationary points with no imaginary frequencies. Gibbs free energies obtained from vibrational analysis were used in the calculation of hydricity, which is defined as the reaction free energy of a compound losing a H-anion. Natural Bond Orbital (NBO) analysis[86] was carried out to calculate the Natural Population Analysis (NPA) atomic charges[87] and Wiberg bond indices (WBIs).[88] All calculations were performed using Gaussian 16, Rev. C01.[89] The wavefunction data of the optimized complexes was then used to perform the Quantum Theory of Atoms-In-Molecules (QTAIM) analysis to obtain the bond critical points (BCPs, or (3, −1) CPs) and AIM charges using the Multiwfn[68] and AIMALL[90] packages. The Cartesian coordinates of all DFT-optimized structures are provided separately as part of the ESI.†

Author contributions

M. M. S. and H. C. designed the project, supervised the research, and authored the manuscript. A. G. G., F. G., E. D., and M. M. S. conducted all synthetic experimentation. A. G. G. and H. C. conducted computational experimentation. K. B. and S. Y. carried out crystallographic experimentation and structure solutions.

Data availability

The data supporting this article have been included as part of the ESI.† Complete details of the X-ray structures can be obtained from the Cambridge Crystallographic Data Centre at **https://www.ccdc.cam.ac.uk**. The CCDC accession numbers for the reported complexes are 2362005, 2362006, 2362008, and 2362009.†

Conflicts of interest

The authors declare no conflicts of interest.

Acknowledgements

A. G. G. acknowledges the Dean's Graduate Fellowship for funding. F. G. acknowledges the Engaged Scholars and Artist Award for funding. M. M. S. acknowledges NSF-CHE-2316582 for financial support of this work. The authors acknowledge the Texas Advanced Computing Center (TACC) under award no. CHE23024 and CHE22010. K. M. B. and S. Y. acknowledge the Cancer Prevention and Research Institute of Texas (Grant No. RR220055) for financial support of this work. Hadi D. Arman is acknowledged for crystallographic assistance. We thank Sergio Gonzalez-Eymard for assistance with IR spectroscopy.

References

1 Q. Wang, S. H. Brooks, T. Liu and N. C. Tomson, *Chem. Commun.*, 2021, **57**, 2839–2853.
2 P. Buchwalter, J. Rosé and P. Braunstein, *Chem. Rev.*, 2015, **115**, 28–126.
3 M. Navarro, J. J. Moreno, M. Pérez-Jiménez and J. Campos, *Chem. Commun.*, 2022, **58**, 11220–11235.
4 J. A. Zurakowski, B. J. Austen and M. W. Drover, *Trends Chem.*, 2022, **4**, 331–346.
5 M. M. Shoshani, *Cell Rep. Phys. Sci.*, 2023, **4**(4), 101213.
6 C. Yoo and Y. Lee, *Chem. Sci.*, 2017, **8**, 600–605.
7 R. C. Cammarota, M. V. Vollmer, J. Xie, J. Ye, J. C. Linehan, S. A. Burgess, A. M. Appel, L. Gagliardi and C. C. Lu, *J. Am. Chem. Soc.*, 2017, **139**, 14244–14250.
8 J. Takaya and N. Iwasawa, *J. Am. Chem. Soc.*, 2017, **139**, 6074–6077.

9 B. L. Ramirez, P. Sharma, R. J. Eisenhart, L. Gagliardi and C. C. Lu, *Chem. Sci.*, 2019, **10**, 3375–3384.
10 R. M. Charles III, T. W. Yokley, N. D. Schley, N. J. DeYonker and T. P. Brewster, *Inorg. Chem.*, 2019, **58**, 12635–12645.
11 B. G. Cooper, J. W. Napoline and C. M. Thomas, *Catal. Rev.*, 2012, **54**, 1–40.
12 B. Wang, C. S. Seo, C. Zhang, J. Chu and N. K. Szymczak, *J. Am. Chem. Soc.*, 2022, **144**, 15793–15802.
13 W.-C. Shih and O. V. Ozerov, *J. Am. Chem. Soc.*, 2017, **139**, 17297–17300.
14 J. A. Zurakowski, B. J. Austen, M. C. Dufour, M. Bhattacharyya, D. M. Spasyuk and M. W. Drover, *Dalton Trans.*, 2021, **50**, 12440–12447.
15 B. E. Cowie and D. J. Emslie, *Organometallics*, 2018, **37**, 1007–1016.
16 L. A. Grose and D. Willcox, *Chem. Commun.*, 2023, **59**, 7427–7430.
17 J. R. Norton and J. Sowa, *Chem. Rev.*, 2016, **116**, 8315–8317.
18 T. Shima, S. Hu, G. Luo, X. Kang, Y. Luo and Z. Hou, *Science*, 2013, **340**, 1549–1552.
19 Y.-X. Luan and M. Ye, *Chem. Commun.*, 2022, **58**, 12260–12273.
20 M. Garçon, A. Phanopoulos, A. J. White and M. R. Crimmin, *Angew. Chem., Int. Ed.*, 2023, **62**, e202213001.
21 Y. Lee, F. T. Sloane, G. Blondin, K. A. Abboud, R. García-Serres and L. J. Murray, *Angew. Chem., Int. Ed.*, 2015, **54**, 1499–1503.
22 Q. Zhao and T. A. Betley, *Angew. Chem., Int. Ed.*, 2011, **50**, 709–712.
23 C. J. Reed and T. Agapie, *J. Am. Chem. Soc.*, 2019, **141**, 9479–9484.
24 M. M. Shoshani, J. Liu and S. A. Johnson, *Organometallics*, 2018, **37**, 116–126.
25 S. Morisako, S. Watanabe, S. Ikemoto, S. Muratsugu, M. Tada and M. Yamashita, *Angew. Chem., Int. Ed.*, 2019, **58**, 15031–15035.
26 L. Escomel, I. Del Rosal, L. Maron, E. Jeanneau, L. Veyre, C. Thieuleux and C. Camp, *J. Am. Chem. Soc.*, 2021, **143**, 4844–4856.
27 O. Ekkert, A. J. White, H. Toms and M. R. Crimmin, *Chem. Sci.*, 2015, **6**, 5617–5622.
28 T. Steinke, C. Gemel, M. Cokoja, M. Winter and R. A. Fischer, *Angew. Chem., Int. Ed.*, 2004, **43**, 2299–2302.
29 N. Gorgas, J. Brünig, B. Stöger, S. Vanicek, M. Tilset, L. F. Veiros and K. Kirchner, *J. Am. Chem. Soc.*, 2019, **141**, 17452–17458.
30 Y. Cai, S. Jiang, T. Rajeshkumar, L. Maron and X. Xu, *J. Am. Chem. Soc.*, 2022, **144**, 16647–16655.
31 Y. Cai, S. Jiang and X. Xu, *Chin. J. Chem.*, 2024, **42**(18), 2133–2139.
32 N. Gorgas, A. J. White and M. R. Crimmin, *J. Am. Chem. Soc.*, 2022, **144**, 8770–8777.
33 N. Gorgas, B. Stadler, A. J. White and M. R. Crimmin, *J. Am. Chem. Soc.*, 2024, **146**(6), 4252–4259.
34 M. Garçon, A. Phanopoulos, G. A. Sackman, C. Richardson, A. J. White, R. I. Cooper, A. J. Edwards and M. R. Crimmin, *Angew. Chem., Int. Ed.*, 2022, **61**, e202211948.
35 T. Steinke, C. Gemel, M. Cokoja, M. Winter and R. A. Fischer, *Angew. Chem., Int. Ed.*, 2004, **43**, 2299–2302.
36 K. R. Pörschke, W. Kleimann, Y. H. Tsay, C. Krüger and G. Wilke, *Chem. Ber.*, 1990, **123**, 1267–1273.
37 B. Pribanic, M. Trincado, F. Eiler, M. Vogt, A. Comas-Vives and H. Grützmacher, *Angew. Chem.*, 2020, **132**, 15733–15739.
38 V. T. Nguyen, Q. Lai, N. Witayapaisitsan, N. Bhuvanesh, P. Surawatanawong and O. V. Ozerov, *Organometallics*, 2023, **42**, 3120–3129.
39 B. J. Graziano, M. V. Vollmer and C. C. Lu, *Angew. Chem.*, 2021, **133**, 15214–15221.
40 E. De Leon, F. Gonzalez, P. Bauskar, S. Gonzalez-Eymard, D. De Los Santos and M. M. Shoshani, *Organometallics*, 2023, **42**, 435–440.
41 N. Hara, K. Semba and Y. Nakao, *ACS Catal.*, 2022, **12**, 1626–1638.
42 M. J. Butler and M. R. Crimmin, *Chem. Commun.*, 2017, **53**, 1348–1365.
43 I. M. Riddlestone, J. A. Abdalla and S. Aldridge, *Adv. Organomet. Chem*, Elsevier, 2015, vol. 63, pp. 1–38.
44 I. M. Riddlestone, S. Edmonds, P. A. Kaufman, J. Urbano, J. I. Bates, M. J. Kelly, A. L. Thompson, R. Taylor and S. Aldridge, *J. Am. Chem. Soc.*, 2012, **134**, 2551–2554.
45 O. Ekkert, A. J. White and M. R. Crimmin, *Angew. Chem., Int. Ed.*, 2016, **55**, 16031–16034.
46 F. Gonzalez, E. De Leon and M. M. Shoshani, *Synlett*, 2024, **35**, A–E.
47 A. Okuniewski, D. Rosiak, J. Chojnacki and B. Becker, *Polyhedron*, 2015, **90**, 47–57.
48 G. Parkin, *Dalton Trans.*, 2022, **51**, 411–427.
49 A. F. Hill, *Organometallics*, 2006, **25**, 4741–4743.
50 R. J. Puddephatt, *Chem. Soc. Rev.*, 1983, **12**, 99–127.
51 N. H. Hunter, E. M. Lane, K. M. Gramigna, C. E. Moore and C. M. Thomas, *Organometallics*, 2021, **40**, 3689–3696.
52 T. Steinke, C. Gemel, M. Cokoja, M. Winter and R. A. Fischer, *Angew. Chem., Int. Ed.*, 2004, **43**, 2299–2302.
53 L. M. Toomey and J. D. Atwood, *Organometallics*, 1997, **16**, 490–493.
54 M. G. Klimpel, R. Anwander, M. Tafipolsky and W. Scherer, *Organometallics*, 2001, **20**, 3983–3992.
55 A. M. Borys, L. A. Malaspina, S. Grabowsky and E. Hevia, *Angew. Chem.*, 2022, **134**, e202209797.
56 A. M. Borys and E. Hevia, *Chimia*, 2023, **77**, 242–242.
57 B. Cordero, V. Gómez, A. E. Platero-Prats, M. Revés, J. Echeverría, E. Cremades, F. Barragán and S. Alvarez, *Dalton Trans.*, 2008, 2832–2838.
58 Y. Ruiz-Morales, G. Schreckenbach and T. Ziegler, *Organometallics*, 1996, **15**, 3920–3923.
59 N. A. Eberhardt and H. Guan, *Chem. Rev.*, 2016, **116**, 8373–8426.
60 W. Liu, Y. Ding, D. Jin, Q. Shen, B. Yan, X. Ma and Z. Yang, *Green Chem.*, 2019, **21**, 3812–3815.

61 C.-C. Chia, Y.-C. Teo, N. Cham, S. Y.-F. Ho, Z.-H. Ng, H.-M. Toh, N. Mézailles and C.-W. So, *Inorg. Chem.*, 2021, **60**, 4569–4577.
62 M. Bhandari, M. Kaur, S. Rawat and S. Singh, *Inorg. Chem.*, 2023, **62**, 6598–6607.
63 C. A. Tolman, *Chem. Rev.*, 1977, **77**, 313–348.
64 G. Ciancaleoni, N. Scafuri, G. Bistoni, A. Macchioni, F. Tarantelli, D. Zuccaccia and L. Belpassi, *Inorg. Chem.*, 2014, **53**, 9907–9916.
65 G. J. Kubas, *Proc. Natl. Acad. Sci. U. S. A.*, 2007, **104**, 6901–6907.
66 L. J. Murphy, H. Hollenhorst, R. McDonald, M. Ferguson, M. D. Lumsden and L. Turculet, *Organometallics*, 2017, **36**, 3709–3720.
67 S. Bajo, M. G. Alférez, M. M. Alcaide, J. López-Serrano and J. Campos, *Chem. – Eur. J.*, 2020, **26**, 16833–16845.
68 T. Lu and F. Chen, *J. Comput. Chem.*, 2012, **33**, 580–592.
69 R. F. W. Bader, *Acc. Chem. Res.*, 1985, **18**, 9–15.
70 M. L. Maiola and J. A. Buss, *Angew. Chem., Int. Ed.*, 2023, **62**, e202311721.
71 J. Hicks, A. Mansikkamäki, P. Vasko, J. M. Goicoechea and S. Aldridge, *Nat. Chem.*, 2019, **11**, 237–241.
72 O. Ekkert, A. J. P. White, H. Toms and M. R. Crimmin, *Chem. Sci.*, 2015, **6**, 5617–5622.
73 S. Banerjee, M. K. Karunananda, S. Bagherzadeh, U. Jayarathne, S. R. Parmelee, G. W. Waldhart and N. P. Mankad, *Inorg. Chem.*, 2014, **53**, 11307–11315.
74 S. Sinhababu, M. R. Radzhabov, J. Telser and N. P. Mankad, *J. Am. Chem. Soc.*, 2022, **144**, 3210–3221.
75 F. Cotton, R. Luck, D. Root and R. Walton, *Inorg. Chem.*, 1990, **29**, 43–47.
76 J. Pursiainen and T. A. Pakkanen, *Acta Chem. Scand.*, 1989, **43**, 463–470.
77 X.-J. Qi, Y. Fu, L. Liu and Q.-X. Guo, *Organometallics*, 2007, **26**, 4197–4203.
78 E. S. Wiedner, M. B. Chambers, C. L. Pitman, R. M. Bullock, A. J. Miller and A. M. Appel, *Chem. Rev.*, 2016, **116**, 8655–8692.
79 M. R. Nimlos, C. H. Chang, C. J. Curtis, A. Miedaner, H. M. Pilath and D. L. DuBois, *Organometallics*, 2008, **27**, 2715–2722.
80 J. R. Prat, R. C. Cammarota, B. J. Graziano, J. T. Moore and C. C. Lu, *Chem. Commun.*, 2022, **58**, 8798–8801.
81 N. Kuhn and T. Kratz, *Synthesis*, 1993, 561–562.
82 J. P. Perdew, *Phys. Rev. B: Condens. Matter Mater. Phys.*, 1986, **33**, 8822.
83 A. D. Becke, *Phys. Rev. A*, 1988, **38**, 3098.
84 F. Weigend, *Phys. Chem. Chem. Phys.*, 2006, **8**, 1057–1065.
85 F. Weigend and R. Ahlrichs, *Phys. Chem. Chem. Phys.*, 2005, **7**, 3297–3305.
86 E. D. Glendening, A. E. Reed, J. E. Carpenter, and F. Weinhold, NBO Version 3.1, Gaussian Inc., Pittsburgh, 2003.
87 A. E. Reed, R. B. Weinstock and F. Weinhold, *J. Chem. Phys.*, 1985, **83**, 735–746.
88 K. B. Wiberg, *Tetrahedron*, 1968, **24**, 1083–1096.
89 M. J. Frisch, G. W. Trucks, H. B. Schlegel, G. E. Scuseria, M. A. Robb, J. R. Cheeseman, G. Scalmani, V. Barone, G. A. Petersson, H. Nakatsuji, X. Li, M. Caricato, A. V. Marenich, J. Bloino, B. G. Janesko, R. Gomperts, B. Mennucci, H. P. Hratchian, J. V. Ortiz, A. F. Izmaylov, J. L. Sonnenberg, D. Williams-Young, F. Ding, F. Lipparini, F. Egidi, J. Goings, B. Peng, A. Petrone, T. Henderson, D. Ranasinghe, V. G. Zakrzewski, J. Gao, N. Rega, G. Zheng, W. Liang, M. Hada, M. Ehara, K. Toyota, R. Fukuda, J. Hasegawa, M. Ishida, T. Nakajima, Y. Honda, O. Kitao, H. Nakai, T. Vreven, K. Throssell, J. A. Montgomery Jr., J. E. Peralta, F. Ogliaro, M. J. Bearpark, J. J. Heyd, E. N. Brothers, K. N. Kudin, V. N. Staroverov, T. A. Keith, R. Kobayashi, J. Normand, K. Raghavachari, A. P. Rendell, J. C. Burant, S. S. Iyengar, J. Tomasi, M. Cossi, J. M. Millam, M. Klene, C. Adamo, R. Cammi, J. W. Ochterski, R. L. Martin, K. Morokuma, O. Farkas, J. B. Foresman and D. J. Fox, *Gaussian 16*, Revision C.01, Gaussian, Inc., Wallingford CT, 2016.
90 T. Keith, **https://aim.tkgristmill.com**.